

Learning to Translate Noise for Robust Image Denoising

Inju Ha^{*1} Donghun Ryou^{*2} Seonguk Seo¹ Bohyung Han^{1,2}
Computer Vision Laboratory, ¹ECE & ²IPAI, Seoul National University

{hij1112, dhryou, seonguk, bhhan}@snu.ac.kr

<https://hij1112.github.io/learning-to-translate-noise/>

Abstract

Deep learning-based image denoising techniques often struggle with poor generalization performance to out-of-distribution real-world noise. To tackle this challenge, we propose a novel noise translation framework that performs denoising on an image with translated noise rather than directly denoising an original noisy image. Specifically, our approach translates complex, unknown real-world noise into Gaussian noise, which is spatially uncorrelated and independent of image content, through a noise translation network. The translated noisy images are then processed by an image denoising network pretrained to effectively remove Gaussian noise, enabling robust and consistent denoising performance. We also design well-motivated loss functions and architectures for the noise translation network by leveraging the mathematical properties of Gaussian noise. Experimental results demonstrate that the proposed method substantially improves robustness and generalizability, outperforming state-of-the-art methods across diverse benchmarks. Visualized denoising results and the source code are available on [our project page](#).

1. Introduction

Image denoising aims to restore the pure signal from noisy images and serves as a critical preprocessing step to improve the visual quality of input images, extending the applicability of various downstream tasks. Recent advances in deep learning have significantly improved the performance of image denoising models [6, 9, 35–40]. A common assumption in early approaches was that camera noise could be modeled as Gaussian noise [23, 39, 40], which simplified the process of generating noisy-clean image pairs by adding synthetic Gaussian noise. This allowed for the creation of large datasets that could be used to train denoising models in a supervised manner, playing a crucial role in advancing the development of denoising models.

Although these models trained on synthetic dataset perform well under controlled environments, they often struggle to generalize to real-world scenarios due to the fundamental differences between synthetic and real noise distributions [9]. In response, researchers have collected clean-noisy image pairs from real images [1, 31, 33] to address realistic noises, but models trained on this data still tend to overfit to the specific noise-signal correlations present in the training data. Capturing the full spectrum of noise distributions in real world images to prevent overfitting is impractical and even unrealistic.

To address this challenge, we propose a novel noise translation framework for image denoising to better generalize to diverse real-world noise using a limited training dataset. The intuition behind our framework is as follows. While existing denoising algorithms trained on images with Gaussian noise exhibit limited performance when applied to real-world noisy images, we observed that adding Gaussian noise to these noisy images significantly improves their effectiveness in denoising, as shown in Figure 1. This observation motivated us to explore the idea that, instead of directly denoising unseen real noise, first translating it into known Gaussian noise and then applying denoising could improve the model’s ability to generalize across unseen out-of-distribution (OOD) noise. To this end, we introduce the lightweight *Noise Translation Network*, which, prior to the denoising process, utilizes Gaussian injection blocks to transform arbitrary complex noise into Gaussian noise that is spatially uncorrelated and independent of an input image. The translated images are then processed by the pretrained denoising networks specialized for Gaussian noise, resulting in the clean denoised images. Once trained, our noise translation network can be seamlessly paired with any denoising network pretrained on Gaussian noise. Our experimental results and analysis validate that the proposed framework outperforms existing denoising approaches by huge margins on various benchmarks.

Our key contributions are summarized as follows:

- We propose a novel noise translation network for robust image denoising, which converts unknown complex noise

^{*} indicates equal contribution.

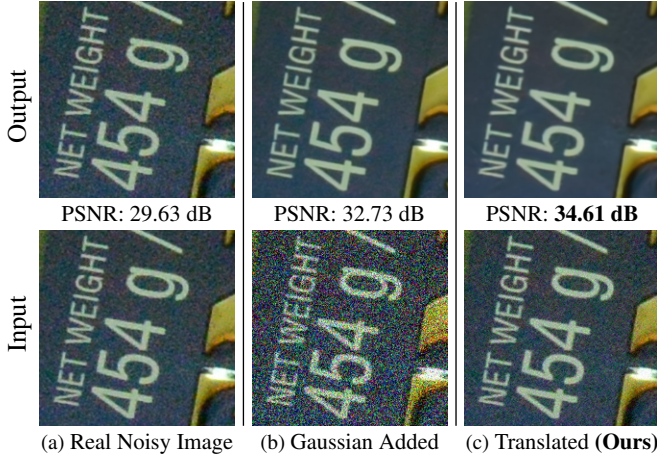


Figure 1. Denoising results of Gaussian-trained Restormer [36], applied to (a) original real noisy image, (b) noisy image with added Gaussian noise. We can observe that simply adding Gaussian noise to a real noisy image improves the denoising performance. (c) showcases our framework which translates real noise into Gaussian noise, enabling the denoising network to achieve even higher quality results. Zoom in for better details.

in an input image into a Gaussian noise. Our lightweight noise translation network can be applied to any Gaussian-pretrained denoising networks.

- We employ well-motivated loss functions and architecture for the noise translation network. The proposed approach guides the noise distribution of the input image to Gaussian distribution both implicitly and explicitly by rigorously leveraging the mathematical properties.
- We demonstrate the efficacy of our approach through extensive experiments on image denoising benchmarks with diverse noise distributions, achieving significant improvements in terms of robustness and generalization ability.

2. Related Works

Image denoising In recent years, deep learning has led to significant progress in image denoising, achieving impressive results by leveraging paired noisy and clean images for training. DnCNN [39] pioneered the use of CNNs for image denoising, which paved the way for further advancements involving residual learning [8, 19, 41], attention mechanisms [18, 41], and transformer models [36, 38]. Despite its success, acquiring the noisy-clean pairs required for supervised training remains a significant challenge. To address this, self-supervised approaches [2, 14, 16, 17, 27] have emerged to train networks using only noisy images, but these models typically perform considerably worse than their supervised counterparts. Additionally, zero-shot approaches [10, 22, 28] have been proposed for image denoising even without training dataset, but they require substantial computational cost at inference, making them impractical for real-time applications. In contrast to these methods

that aim to reduce dependency on supervised data, our approach leverages supervised data but focuses on achieving good generalization performance with limited data.

Generalization for denoising Generalization is a critical challenge in image denoising, as the performance of denoising models often degrades when encountering noise characteristics that were not seen during training. To handle unseen noise type or levels, DnCNN [39] employed blind Gaussian training to adapt to various noise levels, while Mohan *et al.* [25] designed a bias-free network to prevent overfitting to noise levels in the training set. More recent works employed masking-based learning [5] or leveraged the pre-trained CLIP encoder [7] to prevent overfitting by encouraging the model to understand global context rather than relying on local patterns. While these approaches enhance robustness to unseen noise, they often struggle to produce high-quality image restoration, particularly in complex real-world scenarios.

To address real-world noise, researchers have focused on constructing training datasets that closely resemble real noise distribution. This includes collecting real clean-noisy image pairs [1, 31, 33] and learning to generate realistic noise through data augmentation [4, 11, 34] or adversarial attacks [29, 32]. However, these approaches are limited to the noise distributions represented in the training dataset and fail to generalize effectively to unseen OOD noise. Recently, LAN [12] was introduced to address unseen noisy images by applying a learnable pixel-wise offset optimized at test time. However, this approach requires adjusting pixel-level parameters during inference, which limits its scalability as it significantly increases memory and time demands when the input image size is large. In contrast, our framework does not require test-time training, allowing for scalable and efficient denoising at test time.

3. Method

In this section, we present a robust image denoising framework featuring a novel noise translation process, designed to effectively handle diverse unseen noise. Our framework consists of: (1) a noise translation network to transform the arbitrary noise in an input image into ideal Gaussian noise, and (2) a denoising network to remove the translated noise to produce a clean output.

3.1. Image Denoising Network

First of all, we train a denoising network. Our image denoising network aims to recover a clean image from a noisy input, which can be mathematically formulated as

$$\hat{I} = \mathcal{D}(I; \theta), \quad (1)$$

where $\mathcal{D}(\cdot; \theta)$ denotes an image denoising network parameterized by θ , and $I, \hat{I} \in \mathbb{R}^{H \times W \times C}$ represent a noisy input

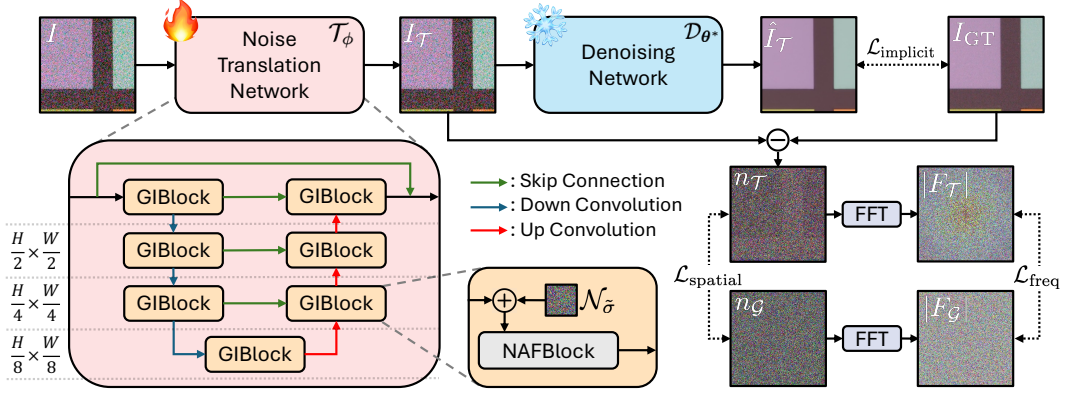


Figure 2. Illustration of our training framework for the noise translation network.

image and its corresponding denoised output, respectively.

The goal of supervised training for our denoising network is to ensure that the denoised output \hat{I} , to closely match the ground-truth clean image I_{GT} . To achieve this, the model parameters θ are optimized by minimizing the following loss function:

$$\mathcal{L} = \|\mathcal{D}(I; \theta) - I_{GT}\|. \quad (2)$$

Our method is model agnostic, allowing us to use existing denoising models and focus only on how to effectively remove Gaussian noise. To train our image denoising network to eliminate Gaussian noise, we utilize a training dataset consisting of clean images paired with their corrupted versions with synthetic additive Gaussian noise. We additionally use Gaussian-augmented real noisy-clean image pairs, where the noisy images are further corrupted with Gaussian noise. In our framework, image denoising network is optimized with the loss function in (2) to make it specialized in removing Gaussian noise.

3.2. Noise Translation Network

Figure 2 illustrates the overall training pipeline of the noise translation network. Formally, our framework first transforms a noisy image I into an image with Gaussian noise I_T , which is then fed into the denoising network to produce the final denoised output \hat{I}_T , represented by

$$\hat{I}_T = \mathcal{D}(I_T; \theta^*) = \mathcal{D}(\mathcal{T}(I; \phi); \theta^*), \quad (3)$$

where $\mathcal{T}(\cdot, \phi)$ denotes the noise translation network with parameters ϕ , and $\mathcal{D}(\cdot, \theta^*)$ indicates the pretrained denoising network with parameters θ^* . Note that $\mathcal{D}(\cdot, \theta^*)$ is specialized in handling Gaussian noise, and its parameters are fixed during training the noise translation network. We next discuss how to train the noise translation network $\mathcal{T}(\cdot, \phi)$ by providing the following two loss terms.

3.2.1. Implicit Noise Translation Loss

Our goal is to transform an arbitrary noisy input image I into a noise-translated image I_T that is well-suited for the

pretrained denoising network, which is specialized for handling Gaussian noise. To achieve this, we optimize the noise translation network using a loss function, referred to as the *implicit* noise translation loss, which is designed to minimize the difference between the denoised image and the ground-truth clean image:

$$\mathcal{L}_{\text{implicit}} = \|\hat{I}_T - I_{GT}\|_1 = \|\mathcal{D}(\mathcal{T}(I; \phi); \theta^*) - I_{GT}\|_1, \quad (4)$$

which guides the network to translate unseen noise into a form that the pretrained denoiser can handle effectively. A straightforward approach to train a noise translation network is to use real noisy-clean image pairs as I and I_{GT} . To handle various noise levels in real-world scenarios that are lacking in the limited training set, we apply data augmentation by adding a random level of synthetic Gaussian noise to the noisy image I . This helps the noise translation network generalize more effectively across diverse noise conditions.

3.2.2. Explicit Noise Translation Loss

The implicit noise translation loss helps to translate the image into a form preferable for the pretrained denoising network, but it does not ensure that the noise distribution is transformed into an ideal Gaussian distribution, as it lacks direct control over the noise characteristics. To address this, we introduce an explicit loss function that directly guides the noise to follow Gaussian distribution.

Let $n_T = I_T - I_{GT} \in \mathbb{R}^{H \times W \times C}$ represent the translated noise, and let $n_G \in \mathbb{R}^{H \times W \times C}$ be a random variable following a Gaussian distribution $\mathcal{N}(\hat{\mu}, \hat{\sigma})$, where $(\hat{\mu}, \hat{\sigma})$ denote the empirical mean and standard deviation calculated from all elements of n_T . Our objective is to adjust the distribution of n_T to closely align with the distribution of n_G . To achieve this, we utilize the Wasserstein distance to measure the difference between their distributions and employ it as a loss function to minimize:

$$\mathcal{L}_{\text{spatial}} \equiv d_{W_1}(n_T, n_G), \quad (5)$$

where $d_{W_1}(\cdot, \cdot)$ is 1-Wasserstein distance, also known as

the Earth Mover’s Distance. To calculate this, we first flatten each channel in $n_{\mathcal{T}}$ and $n_{\mathcal{G}}$ over the spatial dimensions into one-dimensional vectors, and then sort them in an ascending order. Let $\mathbf{X}^c \equiv (X_1^c, X_2^c, \dots, X_{H \times W}^c)$ and $\mathbf{Y}^c \equiv (Y_1^c, Y_2^c, \dots, Y_{H \times W}^c)$ denote the ordered values of $n_{\mathcal{T}}$ and $n_{\mathcal{G}}$ for the c^{th} channel, respectively. The 1-Wasserstein distance is then calculated by the following simple function of the order statistics¹:

$$d_{W_1}(n_{\mathcal{T}}, n_{\mathcal{G}}) = \frac{1}{H \cdot W \cdot C} \sum_{c=1}^C \sum_{i=1}^{H \cdot W} |X_{(i)}^c - Y_{(i)}^c|. \quad (6)$$

This loss encourages the translated noise $n_{\mathcal{T}}$ to follow a Gaussian distribution element-wise, but it is still insufficient to ensure that $n_{\mathcal{T}}$ is spatially uncorrelated. To handle the spatial correlation, we convert the signals of $n_{\mathcal{T}}$ and $n_{\mathcal{G}}$ into the frequency domain using their respective channel-wise Fourier transforms, which are given by

$$F_{\mathcal{T}}^c(u, v) = \sum_{x=0}^{H-1} \sum_{y=0}^{W-1} n_{\mathcal{T}}(x, y, c) e^{-2\pi i(\frac{ux}{H} + \frac{vy}{W})}, \quad (7)$$

$$F_{\mathcal{G}}^c(u, v) = \sum_{x=0}^{H-1} \sum_{y=0}^{W-1} n_{\mathcal{G}}(x, y, c) e^{-2\pi i(\frac{ux}{H} + \frac{vy}{W})}, \quad (8)$$

where (u, v) are the frequency domain coordinates and c is a channel index. Since $n_{\mathcal{G}}$ is spatially uncorrelated Gaussian noise, the real and imaginary parts of the Fourier coefficients, $F_{\mathcal{G}}^c(u, v)$, also follow *i.i.d.* Gaussian distributions with zero mean and the same variance. Consequently, the magnitude of the Fourier coefficients, $|F_{\mathcal{G}}^c(u, v)|$, follows a Rayleigh distribution as

$$p_R(|F_{\mathcal{G}}^c(u, v)|; \sigma) = \frac{|F_{\mathcal{G}}^c(u, v)|}{\sigma^2} \exp\left(-\frac{|F_{\mathcal{G}}^c(u, v)|^2}{2\sigma^2}\right), \quad (9)$$

which implies that $|F_{\mathcal{T}}^c(u, v)|$ should also follow a Rayleigh distribution to ensure that $n_{\mathcal{T}}$ is spatially uncorrelated. To this end, similar to Eqs. (5) and (6), we minimize the difference between the distributions of $|F_{\mathcal{T}}^c(u, v)|$ and $|F_{\mathcal{G}}^c(u, v)|$ by utilizing 1-Wasserstein distance, which is defined as

$$\mathcal{L}_{\text{freq}} \equiv d_{W_1}(|F_{\mathcal{T}}|, |F_{\mathcal{G}}|) = \frac{1}{H \cdot W \cdot C} \sum_{c=1}^C \sum_{i=1}^{H \cdot W} |\tilde{X}_{(i)}^c - \tilde{Y}_{(i)}^c|, \quad (10)$$

where $\tilde{\mathbf{X}}^c \equiv (\tilde{X}_1^c, \tilde{X}_2^c, \dots, \tilde{X}_{H \times W}^c)$ and $\tilde{\mathbf{Y}}^c \equiv (\tilde{Y}_1^c, \tilde{Y}_2^c, \dots, \tilde{Y}_{H \times W}^c)$ are the sorted values of flattened magnitude of Fourier coefficients $|F_{\mathcal{T}}^c(u, v)|$ and $|F_{\mathcal{G}}^c(u, v)|$, respectively.

The full explicit noise translation loss is defined by $\mathcal{L}_{\text{spatial}}$ and $\mathcal{L}_{\text{freq}}$ as

$$\mathcal{L}_{\text{explicit}} = \mathcal{L}_{\text{spatial}} + \beta \cdot \mathcal{L}_{\text{freq}}, \quad (11)$$

¹Please refer to Appendix for the detailed proof.

where β is a hyperparameter that balances the contribution of the two Wasserstein distances. This loss function explicitly guides the translated noise to follow Gaussian distribution.

The total loss function for training the noise translation network is given by

$$\mathcal{L}_{\text{total}} = \mathcal{L}_{\text{implicit}} + \alpha \cdot \mathcal{L}_{\text{explicit}}, \quad (12)$$

where α is a hyperparameter to control the influence of implicit and explicit loss terms.

3.2.3. Gaussian Injection Block

As illustrated in Figure 2, our noise translation network is built upon a lightweight U-Net architecture, where each layer is composed of Gaussian Injection Blocks (GIBlock). GIBlock incorporates a Nonlinear Activation-Free (NAF) block from NAFNet [6] along with our key idea to align the discrepancy between training and inference stage: Gaussian noise injection.

In the training stage of noise translation network, random levels of Gaussian noise is augmented to an input image I to address diverse noise conditions, enhancing the robustness of the noise translation network. In contrast, in inference stage, noisy input images are given directly to the noise translation network without adding extra Gaussian noise, because the direct noise augmentation to the input images degrades output quality. To establish a consistent Gaussian noise prior in both the training and inference stage, we inject Gaussian noise into every intermediate block of the noise translation network. Since the noise translation network is designed based on U-Net with residual connections between the input I and the output $I_{\mathcal{T}}$, the distortion of the signal caused by injected Gaussian noise is alleviated, while allowing the noise translation network to utilize the Gaussian prior for transforming unseen real noise. Our ablation studies further demonstrate that the proposed Gaussian noise injection is crucial for the noise translation network to effectively translate unseen noise into Gaussian noise during the inference stage.

4. Experiments

We demonstrate the effectiveness of the proposed approach on various benchmarks, evaluating performance and conducting analysis on both ID and OOD datasets. This section also provides an in-depth analysis of our algorithm, including detailed ablation studies and qualitative assessments.

4.1. Experimental Settings

Training details Since our approach is model-agnostic, we employ existing architectures such as NAFNet [6], Restormer [36], KBNNet [42] and Xformer [38] as our image denoising network, which is pretrained on BSD400 [24], WED [21], and SIDD medium [1] datasets. BSD400 and

Table 1. Quantitative comparison between other state-of-the-art real-world denoising networks and our framework-applied networks on the SIDD validation set and various out-of-distribution (OOD) real-world benchmarks. The results are presented in terms of PSNR \uparrow (dB) and SSIM \uparrow . Models marked with an asterisk (*) are evaluated using official out-of-the-box models.

Denoising Method	Metric	In-distribution			Out-of-distribution						
		SIDD	Poly	CC	HighISO	iPhone	Huawei	OPPO	Sony	Xiaomi	OOD Avg.
R2R* [27]	PSNR	35.06	36.81	35.26	37.33	39.19	38.29	39.32	41.46	35.36	37.88
	SSIM	0.9150	0.9722	0.9756	0.9712	0.9606	0.9663	0.9739	0.9729	0.9664	0.9699
AP-BSN* [15]	PSNR	36.32	35.88	33.13	36.66	39.82	37.01	39.04	40.04	33.37	36.87
	SSIM	0.9281	0.9751	0.9732	0.9777	0.9766	0.9628	0.9746	0.9798	0.9548	0.9718
SSID* [17]	PSNR	37.39	37.13	34.93	38.24	40.85	37.22	39.10	42.89	34.25	38.08
	SSIM	0.9338	0.9799	0.9805	0.9808	0.9816	0.9652	0.9738	0.9878	0.9562	0.9757
Restormer* [36]	PSNR	39.93	37.63	36.31	38.24	40.05	38.36	39.49	44.02	35.62	38.85
	SSIM	0.9598	0.9790	0.9805	0.9753	0.9727	0.9671	0.9768	0.9889	0.9706	0.9745
Restormer-ours	PSNR	39.08	38.74	37.60	40.06	41.62	39.68	40.55	44.12	36.14	39.81
	SSIM	0.9558	0.9846	0.9861	0.9851	0.9751	0.9761	0.9794	0.9849	0.9747	0.9807
NAFNet* [6]	PSNR	39.88	37.13	35.81	38.27	40.16	37.68	39.57	43.48	34.97	38.38
	SSIM	0.9594	0.9714	0.9809	0.9784	0.9700	0.9676	0.9781	0.9824	0.9681	0.9746
NAFNet-ours	PSNR	39.17	38.67	37.82	39.94	41.94	39.74	40.45	44.17	36.14	39.86
	SSIM	0.9566	0.9851	0.9876	0.9853	0.9805	0.9778	0.9796	0.9869	0.9745	0.9822
KBNet* [42]	PSNR	40.26	36.79	35.21	38.05	37.93	35.14	37.73	41.65	34.23	37.09
	SSIM	0.9618	0.9785	0.9808	0.9785	0.9526	0.9459	0.9657	0.9784	0.9640	0.9681
KBNet-ours	PSNR	39.06	38.57	37.59	39.83	41.63	39.71	40.46	44.04	36.04	39.73
	SSIM	0.9559	0.9840	0.9859	0.9845	0.9752	0.9773	0.9794	0.9839	0.9739	0.9805
XFormer* [38]	PSNR	39.89	37.41	35.93	37.82	39.92	38.30	39.54	43.74	35.52	38.52
	SSIM	0.9599	0.9774	0.9781	0.9738	0.9725	0.9673	0.9773	0.9886	0.9702	0.9756
XFormer-ours	PSNR	38.98	38.67	37.73	40.22	42.04	39.79	40.61	44.26	36.23	39.94
	SSIM	0.9549	0.9852	0.9857	0.9857	0.9816	0.9773	0.9805	0.9879	0.9748	0.9824

WED datasets consist of clean images, while SIDD dataset is composed of real noisy-clean image pairs. During the training of a denoising network, noisy images are created by adding Gaussian noise with a standard deviation of 15 to clean images from the BSD400 and WED datasets, or to different formats of noisy images from the SIDD dataset. Each training batch consists of images drawn equally from two sources: half from the BSD400 and WED datasets, and the other half from the SIDD dataset. The denoising models are trained for 200K iterations with a batch size of 32, except for Restormer and Xformer, where the batch size is reduced to 4 due to the limitation of computational resources. The noise translation network is trained subsequently, with the noisy images from the SIDD dataset augmented by adding stochastic level of Gaussian noise with a range of 0 to 15. The noise translation network is trained for 5K iterations with a batch size of 4. Denoising network and noise translation network are trained with the AdamW [20] optimizer with an initial learning rate of 10^{-3} , which is reduced to 10^{-7} and 10^{-5} by a cosine annealing schedule, respectively. Each image is randomly cropped to 256×256 for training. The hyperparameters in our experiment are set as follows: a Gaussian noise injection level $\tilde{\sigma} = 100$,

$\alpha = 5 \times 10^{-2}$, and $\beta = 2 \times 10^{-3}$. All trainings were conducted using two NVIDIA RTX A6000 GPUs.

Evaluation To evaluate the generalization performance of our framework, we employ various real-world image denoising benchmarks. We conduct experiments using SIDD validation dataset [1], Poly [31], CC [26], HighISO [33], iPhone, Huawei, Oppo, Sony, and Xiaomi [13]. The SIDD validation dataset consists of images with a resolution of 256×256 pixels, while the Poly and CC datasets contain images with a resolution of 512×512 pixels. Images from HighISO, iPhone, Huawei, Oppo, Sony, and Xiaomi are 1024×1024 pixels in size.

4.2. Results

Denoising performance on real noise Table 1 presents the performance of the proposed approach applied to the denoising networks, including Restormer [36], NAFNet [6], KBNet [42], and Xformer [38], alongside results from self-supervised image denoising methods, including R2R [27], AP-BSN [15], and SSID [17] for comparison. For evaluating existing methods, we use the officially published models trained on the SIDD dataset, where self-supervised methods

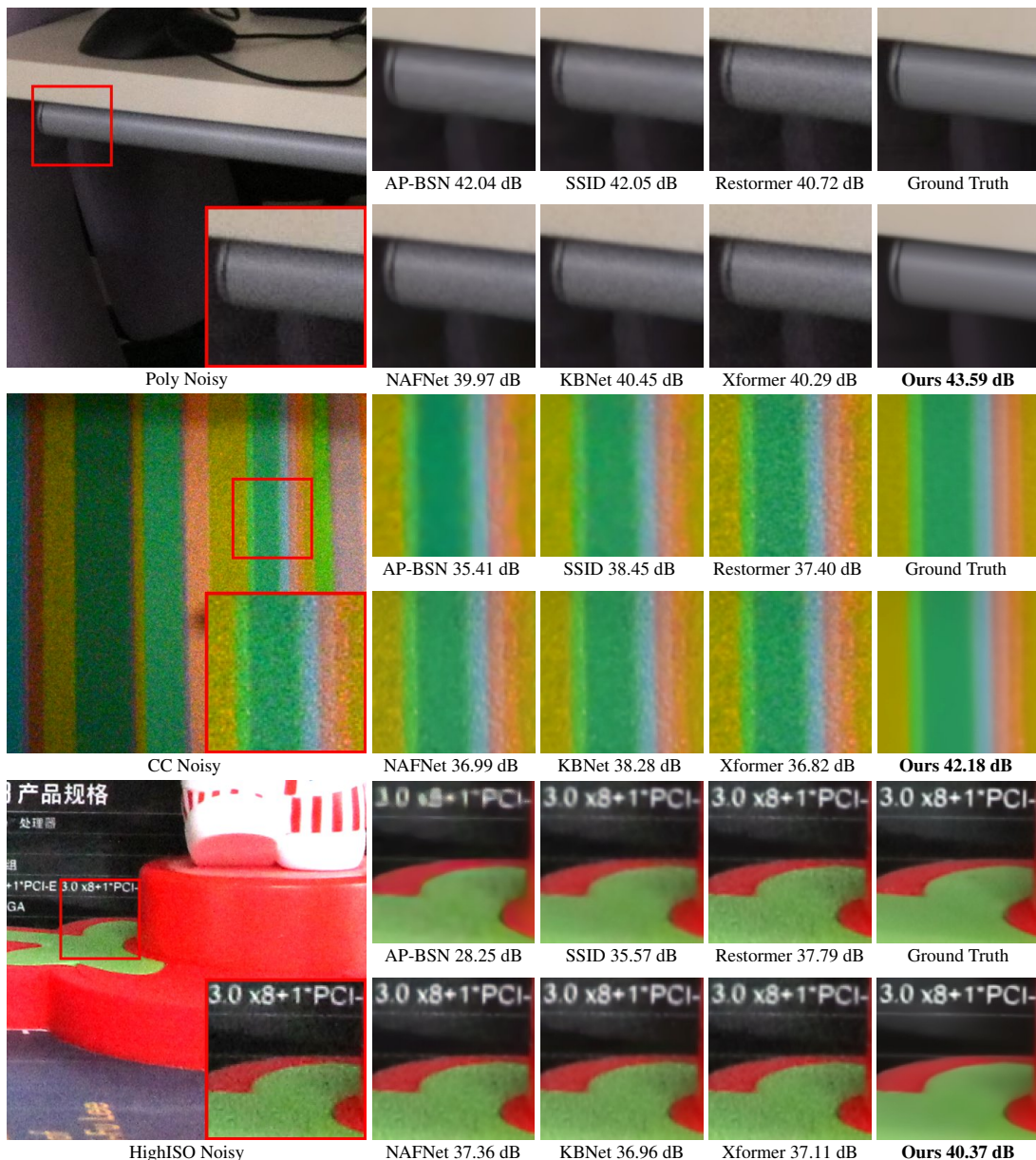


Figure 3. Comparison between the qualitative results of various denoising networks including ours (noise translation network with pre-trained NAFNet), on the out-of-distribution (OOD) datasets. Our result displays cleaner outputs compared to other state-of-the-art networks trained on a real-noise dataset with self-supervised and supervised methods.

are trained with only noisy images. As shown in Table 1, incorporating our noise translation framework—denoted by Restormer-ours, NAFNet-ours, KBNets-ours, and Xformer-ours—yields significant average PSNR improvements of 0.96dB, 1.48dB, 2.64dB, and 1.42dB, respectively, in out-of-distribution (OOD) scenarios. This demonstrates the effectiveness of our method in enhancing the generalization performance of real-world image denoising networks. Additional comparisons with recent studies on generalizable denoising, including LAN [12] and AFM [29], are presented in the Appendix.

Qualitative results on OOD benchmarks Figure 3 illustrates qualitative results for denoising models on several real-world OOD datasets, including Poly [31], CC [26], and HighISO [33]. Our model demonstrates significant superiority over other denoising methods in these challenging scenarios. Additional qualitative results on every benchmark listed in Table 1 are available in the Appendix.

4.3. Analysis

We perform a comprehensive analysis using the noise translation network with pretrained NAFNet (NAFNet-ours).

Table 2. Quantitative results based on variations in the noisy input to the pretrained denoising network on the SIDD validation set (in-distribution) and other real-world benchmarks (out-of-distribution). I , $I + \mathcal{N}_5$, $I + \mathcal{N}_{10}$, and $I + \mathcal{N}_{15}$ represent the noisy input images with additional Gaussian noise levels of 0, 5, 10, and 15, respectively, which are fed into the pretrained Gaussian denoising network. We present performance in terms of PSNR \uparrow (dB) and SSIM \uparrow .

Input	Metric	In-distribution				Out-of-distribution					
		SIDD	Poly	CC	HighISO	iPhone	Huawei	OPPO	Sony	Xiaomi	OOD Avg.
I	PSNR	37.77	15.24	33.76	21.18	40.13	8.68	8.45	6.35	9.33	17.89
	SSIM	0.9360	0.3466	0.9139	0.5232	0.9734	0.1218	0.1138	0.0245	0.1845	0.4002
$I + \mathcal{N}_5$	PSNR	38.15	27.07	34.97	32.30	15.28	16.99	13.79	12.82	14.96	22.93
	SSIM	0.9436	0.7010	0.9211	0.8227	0.2392	0.3943	0.2564	0.1912	0.3540	0.5359
$I + \mathcal{N}_{10}$	PSNR	38.76	38.27	37.33	39.40	40.95	39.44	39.98	42.96	35.91	39.22
	SSIM	0.9536	0.9795	0.9850	0.9825	0.9638	0.9762	0.9768	0.9758	0.9728	0.9740
$I + \mathcal{N}_{15}$	PSNR	39.16	38.08	36.26	38.85	41.12	38.71	39.69	43.42	35.25	38.95
	SSIM	0.9565	0.9834	0.9829	0.9808	0.9811	0.9719	0.9770	0.9886	0.9680	0.9767
$I_{\mathcal{T}}$	PSNR	39.17	38.67	37.82	39.94	41.94	39.74	40.45	44.17	36.14	39.86
	SSIM	0.9566	0.9851	0.9876	0.9853	0.9805	0.9778	0.9796	0.9869	0.9745	0.9822

Table 3. Effects of using Gaussian injection block and explicit noise translation loss. The results for each OOD dataset are detailed in the Appendix.

	Metric	SIDD	OOD Avg.
Baseline Translation	PSNR	39.35	39.27
	SSIM	0.9573	0.9774
+ Gaussian Injection Block	PSNR	39.05	39.61
	SSIM	0.9556	0.9801
+ Explicit Noise Translation Loss	PSNR	39.37	38.66
	SSIM	0.9574	0.9720
+ Both (Ours)	PSNR	39.17	39.86
	SSIM	0.9566	0.9822

Comparisons with simple Gaussian noise additions We assess the effectiveness of our noise translation network by comparing it to simply adding Gaussian noise to the input. As shown in table 2, adding Gaussian noise to the input achieve reasonable generalization performance. However, some datasets perform better with an input of $I + \mathcal{N}_{10}$, while others perform better with $I + \mathcal{N}_{15}$. This variation suggests that each image or dataset exhibits distinct noise characteristics, highlighting the need for a more adaptable approach than applying a fixed level of Gaussian noise. Our noise translation network flexibly transforms the input noise of each image into ideal Gaussian noise, resulting in significant performance improvements across all datasets.

Gaussian injection and explicit noise translation loss

Table 3 illustrates the performance gains attributed to each component of the proposed method. The baseline translation in Table 3 refers to the results obtained by applying our method without Gaussian noise injection and explicit noise translation loss. We observe the best performance

Table 4. Quantitative results to demonstrate the adaptability of our noise translation framework. The metrics for each OOD dataset are presented in the Appendix.

$\mathcal{D}_{\theta^*} - train$	$\mathcal{D}_{\theta^*} - test$	Metric	SIDD	OOD Avg.
NAFNet [6]	Restormer [36]	PSNR	39.19	39.75
		SSIM	0.9567	0.9820
	KBNet [42]	PSNR	39.15	39.84
		SSIM	0.9565	0.9819
Xformer [38]	PSNR	39.02	39.84	
	SSIM	0.9555	0.9822	

gains when both Gaussian noise injection and explicit noise translation loss are both applied.

Adaptability of the noise translation network In our framework, the noise translation network and the denoising network perform distinct tasks, enabling the use of a single noise translation network with different pretrained denoising networks. Table 4 demonstrates the flexibility by applying a noise translation network trained with pretrained NAFNet [6] to other architectures: Restormer [36], KBNet [42], and Xformer [38]. The results show comparable performance to using a noise translation network specifically trained for each denoising model, reported in Table 1. This suggests that a single-time trained noise translation network can be employed with various pretrained denoising networks, without a necessary additional training.

Analysis of translated noise Figure 4 visualizes the results of our noise translation process. Real noise exhibits strong spatial correlation and signal dependency. Our noise translation network effectively alleviates these characteristics, converting the noise into a form that resembles ideal

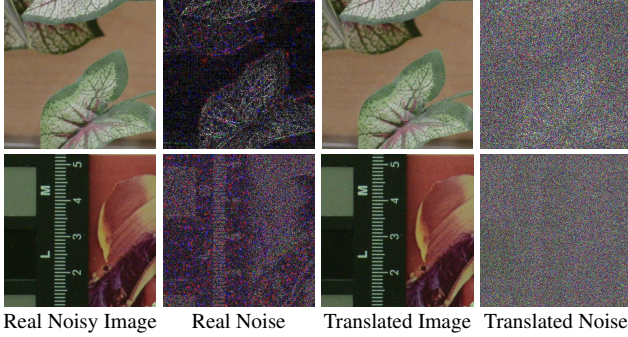


Figure 4. Visual results of noise translation. The noisy image in the top row is from the Poly [31] dataset, while the one in the bottom row is from the CC [26] dataset. For enhanced visualization, noise is displayed as the absolute value, scaled by a factor of 10.

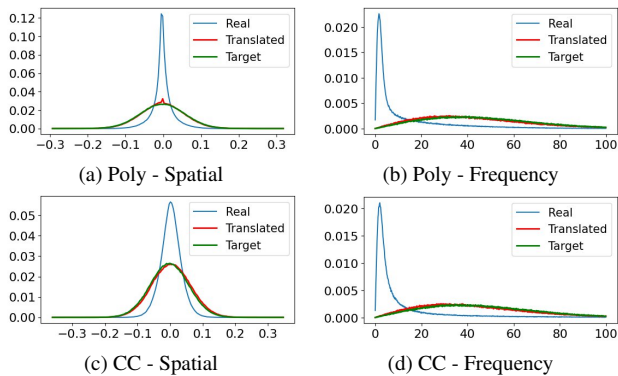


Figure 5. Histogram of noise distribution before (Real) and after noise translation network in both spatial and frequency domains. Target noise corresponds to the Gaussian noise with a level of 15, which the denoising network has been pretrained to remove.

Gaussian noise. Figure 5 presents the analysis of the noise distribution of two images dealt in Figure 4. In the spatial domain, ideal Gaussian noise follow a normal distribution, while in the frequency domain, it follows Rayleigh distribution, as discussed in Section 3.2.2. The original real-noise distribution significantly deviates from the expected target. After the translation, the noise closely matches the target distributions, demonstrating the effectiveness of our method in aligning the noise with spatially uncorrelated, *i.i.d* Gaussian noise.

Evaluating Trade-offs in ID Performance Figure 6 displays an enlarged qualitative results on the SIDD validation dataset. Although our method may seem to show a trade-off in in-distribution (ID) performance, this is primarily attributed to the pronounced overfitting of other models, which often reconstruct irrelevant artifacts inherent in the training data. In contrast, our approach preserves high visual quality while avoiding overfitting, effectively removing noise without introducing such artifacts.

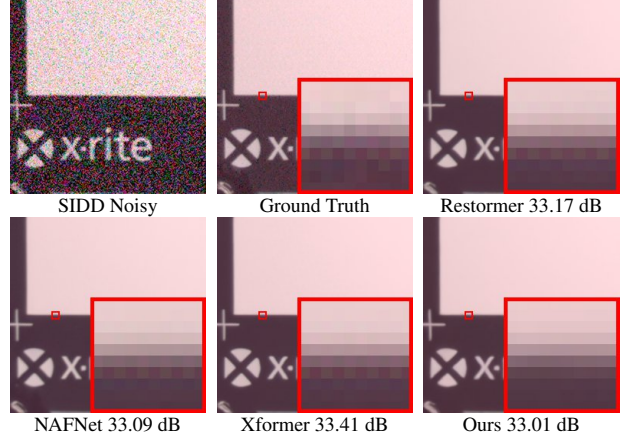


Figure 6. Denoised results of an in-distribution SIDD [1] noisy image. Only our approach effectively avoids overfitting, preventing unnecessary zipper artifacts prevalent in the training set, while preserving the visual quality. Zoom in for detailed comparison.

Table 5. Parameter counts and MACs of denoising networks and our noise translation network. We report the number of parameters and MACs at inference, estimated with an input size of 256×256 .

Architecture	Parameters (M)	MACs (G)
NAFNet [6]	29.10	16.23
Restormer [36]	26.13	140.99
KBNet [42]	104.93	58.19
Xformer [38]	25.12	142.68
Noise Translation Network	0.29	1.07

Computational efficiency Table 5 presents a comparison of our noise translation network with other image denoising networks in terms of the number of parameters and multiply-accumulate operations (MACs). Our noise translation network is significantly smaller in size compared to the image denoising networks, resulting in negligible additional computational cost during inference.

5. Conclusion

We presented a novel noise translation framework for robust image denoising. Our framework allows us to effectively remove various unseen real noise, even with limited amount of training data. By employing the noise translation network, we transform arbitrary out-of-distribution (OOD) noise into Gaussian noise for which our image denoising network has learned during training. The noise translation network is designed with well-motivated loss functions and architecture, enabling effective noise translation while preserving image contents. Our experiments demonstrate that the proposed approach significantly outperforms state-of-the-art denoising models in diverse OOD real-noise benchmarks. Finally, we highlight that the generalization issue remains a critical challenge in image denoising, and our approach offers a promising solution.

References

- [1] Abdelrahman Abdelhamed, Stephen Lin, and Michael S Brown. A high-quality denoising dataset for smartphone cameras. In *CVPR*, 2018. 1, 2, 4, 5, 8
- [2] Joshua Batson and Loic Royer. Noise2self: Blind denoising by self-supervision. In *ICML*. PMLR, 2019. 2
- [3] Benoit Brummer and Christophe De Vleeschouwer. Natural image noise dataset. In *Proceedings of the IEEE/CVF Conference on Computer Vision and Pattern Recognition (CVPR) Workshops*, 2019. 15
- [4] Yuanhao Cai, Xiaowan Hu, Haoqian Wang, Yulun Zhang, Hanspeter Pfister, and Donglai Wei. Learning to generate realistic noisy images via pixel-level noise-aware adversarial training. *NIPS*, 34, 2021. 2, 12
- [5] Haoyu Chen, Jinjin Gu, Yihao Liu, Salma Abdel Magid, Chao Dong, Qiong Wang, Hanspeter Pfister, and Lei Zhu. Masked image training for generalizable deep image denoising. In *CVPR*, 2023. 2, 12
- [6] Liangyu Chen, Xiaojie Chu, Xiangyu Zhang, and Jian Sun. Simple baselines for image restoration. In *ECCV*, 2022. 1, 4, 5, 7, 8, 12, 14
- [7] Jun Cheng, Dong Liang, and Shan Tan. Transfer clip for generalizable image denoising. In *CVPR*, 2024. 2, 12
- [8] Shuhang Gu, Yawei Li, Luc Van Gool, and Radu Timofte. Self-guided network for fast image denoising. In *ICCV*, 2019. 2
- [9] Shi Guo, Zifei Yan, Kai Zhang, Wangmeng Zuo, and Lei Zhang. Toward convolutional blind denoising of real photographs. In *CVPR*, 2019. 1
- [10] Tao Huang, Songjiang Li, Xu Jia, Huchuan Lu, and Jianzhuang Liu. Neighbor2neighbor: Self-supervised denoising from single noisy images. In *CVPR*, 2021. 2
- [11] Geonwoon Jang, Wooseok Lee, Sanghyun Son, and Kyoung Mu Lee. C2n: Practical generative noise modeling for real-world denoising. In *ICCV*, 2021. 2, 12
- [12] Changjin Kim, Tae Hyun Kim, and Sungyong Baik. Lan: Learning to adapt noise for image denoising. In *CVPR*, 2024. 2, 6, 12
- [13] Zhaoming Kong, Fangxi Deng, Haomin Zhuang, Jun Yu, Lifang He, and Xiaowei Yang. A comparison of image denoising methods, 2023. 5
- [14] Alexander Krull, Tim-Oliver Buchholz, and Florian Jug. Noise2void-learning denoising from single noisy images. In *CVPR*, 2019. 2
- [15] Wooseok Lee, Sanghyun Son, and Kyoung Mu Lee. Ap-bsn: Self-supervised denoising for real-world images via asymmetric pd and blind-spot network. In *CVPR*, 2022. 5
- [16] Jaakko Lehtinen, Jacob Munkberg, Jon Hasselgren, Samuli Laine, Tero Karras, Miika Aittala, and Timo Aila. Noise2noise: Learning image restoration without clean data. *ICML*, 2018. 2
- [17] Junyi Li, Zhilu Zhang, Xiaoyu Liu, Chaoyu Feng, Xiaotao Wang, Lei Lei, and Wangmeng Zuo. Spatially adaptive self-supervised learning for real-world image denoising. In *CVPR*, 2023. 2, 5
- [18] Ding Liu, Bihan Wen, Yuchen Fan, Chen Change Loy, and Thomas S Huang. Non-local recurrent network for image restoration. In *NIPS*, 2018. 2
- [19] Xing Liu, Masanori Suganuma, Zhun Sun, and Takayuki Okatani. Dual residual networks leveraging the potential of paired operations for image restoration. In *CVPR*, 2019. 2
- [20] Ilya Loshchilov and Frank Hutter. Decoupled weight decay regularization. In *ICLR*, 2019. 5
- [21] Kede Ma, Zhengfang Duanmu, Qingbo Wu, Zhou Wang, Hongwei Yong, Hongliang Li, and Lei Zhang. Waterloo exploration database: New challenges for image quality assessment models. *IEEE Transactions on Image Processing*, 26(2), 2016. 4
- [22] Youssef Mansour and Reinhard Heckel. Zero-shot noise2noise: Efficient image denoising without any data. In *CVPR*, 2023. 2
- [23] Xiaojiao Mao, Chunhua Shen, and Yu-Bin Yang. Image restoration using very deep convolutional encoder-decoder networks with symmetric skip connections. In *NIPS*, 2016. 1
- [24] David Martin, Charless Fowlkes, Doron Tal, and Jitendra Malik. A database of human segmented natural images and its application to evaluating segmentation algorithms and measuring ecological statistics. In *ICCV*. IEEE, 2001. 4
- [25] Sreyas Mohan, Zahra Kadkhodaie, Eero P. Simoncelli, and Carlos Fernandez-Granda. Robust and interpretable blind image denoising via bias-free convolutional neural networks. In *ICLR*, 2020. 2
- [26] Seonghyeon Nam, Youngbae Hwang, Yasuyuki Matsushita, and Seon Joo Kim. A holistic approach to cross-channel image noise modeling and its application to image denoising. In *CVPR*, 2016. 5, 6, 8
- [27] Tongyao Pang, Huan Zheng, Yuhui Quan, and Hui Ji. Recorrupted-to-recorrupted: unsupervised deep learning for image denoising. In *CVPR*, 2021. 2, 5
- [28] Yuhui Quan, Mingqin Chen, Tongyao Pang, and Hui Ji. Self2self with dropout: Learning self-supervised denoising from single image. In *CVPR*, 2020. 2
- [29] Donghun Ryou, Inju Ha, Hyewon Yoo, Dongwan Kim, and Bohyung Han. Robust image denoising through adversarial frequency mixup. In *CVPR*, 2024. 2, 6, 12
- [30] C. Villani and American Mathematical Society. *Topics in Optimal Transportation*. American Mathematical Society, 2003. 11
- [31] Jun Xu, Hui Li, Zhetong Liang, David Zhang, and Lei Zhang. Real-world noisy image denoising: A new benchmark. *arXiv preprint arXiv:1804.02603*, 2018. 1, 2, 5, 6, 8
- [32] Hanshu Yan, Jingfeng Zhang, Jiashi Feng, Masashi Sugiyama, and Vincent YF Tan. Towards adversarially robust deep image denoising. In *IJCAI*, 2022. 2
- [33] Huanjing Yue, Jianjun Liu, Jingyu Yang, Truong Q Nguyen, and Feng Wu. High iso jpeg image denoising by deep fusion of collaborative and convolutional filtering. *IEEE Transactions on Image Processing*, 28(9), 2019. 1, 2, 5, 6
- [34] Zongsheng Yue, Qian Zhao, Lei Zhang, and Deyu Meng. Dual adversarial network: Toward real-world noise removal and noise generation. In *ECCV*, 2020. 2, 12

- [35] Syed Waqas Zamir, Aditya Arora, Salman Khan, Munawar Hayat, Fahad Shahbaz Khan, Ming-Hsuan Yang, and Ling Shao. Learning enriched features for real image restoration and enhancement. In *ECCV*. Springer, 2020. 1
- [36] Syed Waqas Zamir, Aditya Arora, Salman Khan, Munawar Hayat, Fahad Shahbaz Khan, and Ming-Hsuan Yang. Restormer: Efficient transformer for high-resolution image restoration. In *CVPR*, 2022. 2, 4, 5, 7, 8, 12, 14
- [37] Syed Waqas Zamir, Aditya Arora, Salman Khan, Munawar Hayat, Fahad Shahbaz Khan, Ming-Hsuan Yang, and Ling Shao. Learning enriched features for fast image restoration and enhancement. *IEEE transactions on pattern analysis and machine intelligence*, 45(2), 2022.
- [38] Jiale Zhang, Yulun Zhang, Jinjin Gu, Jiahua Dong, Linghe Kong, and Xiaokang Yang. Xformer: Hybrid x-shaped transformer for image denoising. In *ICLR*, 2024. 2, 4, 5, 7, 8, 12
- [39] Kai Zhang, Wangmeng Zuo, Yunjin Chen, Deyu Meng, and Lei Zhang. Beyond a gaussian denoiser: Residual learning of deep cnn for image denoising. *IEEE transactions on image processing*, 26(7), 2017. 1, 2
- [40] Kai Zhang, Wangmeng Zuo, and Lei Zhang. Ffdnet: Toward a fast and flexible solution for cnn-based image denoising. *IEEE Transactions on Image Processing*, 27(9), 2018. 1
- [41] Yulun Zhang, Kungpeng Li, Kai Li, Bineng Zhong, and Yun Fu. Residual non-local attention networks for image restoration. In *ICLR*, 2019. 2
- [42] Yi Zhang, Dasong Li, Xiaoyu Shi, Dailan He, Kangning Song, Xiaogang Wang, Honwei Qin, and Hongsheng Li. Kbnnet: Kernel basis network for image restoration. *arXiv preprint arXiv:2303.02881*, 2023. 4, 5, 7, 8, 12, 15

Appendix:

Learning to Translate Noise for Robust Image Denoising

A. Proof on Wasserstein Distance

Let P and Q represent two probability distributions over \mathbb{R}^d . We use $X \sim P$ and $Y \sim Q$ to denote random variables with the distributions P and Q , respectively. The p -Wasserstein distance between two probability measures P and Q is defined as follows:

$$W_p(P, Q) = \left(\inf_{J \in \mathcal{J}(P, Q)} \int \|x - y\|^p dJ(x, y) \right)^{1/p}, \quad (\text{S.1})$$

where $\mathcal{J}(P, Q)$ is the set of all joint distributions (or couplings) J on (X, Y) that have marginals P and Q . This formulation describes the minimum cost of transporting mass from distribution P to distribution Q using the coupling J , with the cost measured as the p -th power of the distance between points x and y .

In the Monge formulation, the goal is to find a transport map $T : \mathbb{R}^d \rightarrow \mathbb{R}^d$ such that the push-forward of P under T , denoted as $T_{\#}P$, equals Q . This problem can be mathematically formulated as:

$$\inf_T \int |x - T(x)|^p dP(x), \quad (\text{S.2})$$

where the map T moves the distribution P to Q . However, an optimal map T may not always exist. In such cases, the Kantorovich formulation is used, allowing mass at each point to be split and transported to multiple locations, leading to a coupling-based approach.

For the specific case of $p = 1$, known as the Earth Mover's Distance, the dual formulation of the Wasserstein distance can be expressed as:

$$W_1(P, Q) = \sup_{f \in F} \left(\int f(x) dP(x) - \int f(x) dQ(x) \right), \quad (\text{S.3})$$

where F represents the set of all Lipschitz continuous functions $f : \mathbb{R}^d \rightarrow \mathbb{R}$ such that $|f(y) - f(x)| \leq \|x - y\|$ for all $x, y \in \mathbb{R}^d$. Then, the 1-Wasserstein distance is given by:

$$W_1(P, Q) = \int_0^1 |F^{-1}(z) - G^{-1}(z)| dz, \quad (\text{S.4})$$

where F^{-1} and G^{-1} denote the quantile functions (inverse CDFs) of P and Q , respectively.

When P and Q are empirical distributions based on the datasets, X_1, X_2, \dots, X_n and Y_1, Y_2, \dots, Y_n , each of size n , the Wasserstein distance can be computed as a function of the order statistics:

$$W_1(P, Q) = \sum_{i=1}^n |X_{(i)} - Y_{(i)}|, \quad (\text{S.5})$$

where $X_{(i)}$ and $Y_{(i)}$ denote the i -th order statistics of the datasets X_1, X_2, \dots, X_n and Y_1, Y_2, \dots, Y_n .

In our approach, we utilize (S.5) to formulate $\mathcal{L}_{\text{spatial}}$ in Eq. (5) and $\mathcal{L}_{\text{freq}}$ in Eq. (10), which are employed during training to explicitly transport the translated noise distribution towards the target Gaussian distribution. We refer to [30] for a detailed discussion on Wasserstein distances and optimal transport.

Table S.1. Quantitative comparison of additional state-of-the-art image denoising methods on the SIDD validation set and multiple real-noise benchmarks. We present the results in terms of PSNR \uparrow (dB) and SSIM \uparrow . Methods marked with an asterisk (*) are evaluated using official out-of-the-box models.

Denoising method		Metric	SIDD	Poly	CC	HighISO	iPhone	Huawei	OPPO	Sony	Xiaomi	Total Avg.
GAN-based	DANet* [34]	PSNR	39.47	37.53	36.16	38.35	40.46	38.40	39.85	44.36	35.57	38.90
		SSIM	0.9570	0.9800	0.9815	0.9770	0.9751	0.9691	0.9789	0.9895	0.9706	0.9754
	C2N + DIDN* [11]	PSNR	35.36	37.60	36.92	38.82	40.48	38.56	40.08	44.63	35.44	38.65
		SSIM	0.9321	0.9781	0.9813	0.9765	0.9745	0.9679	0.9793	0.9899	0.9684	0.9720
	PNGAN + MIRNet* [4]	PSNR	39.98	37.41	36.10	38.24	39.93	38.02	39.56	43.15	35.24	38.62
		SSIM	0.959	0.9783	0.9810	0.9763	0.9711	0.9678	0.9782	0.9860	0.9690	0.9741
Others	MaskDenoising* [5]	PSNR	28.66	34.56	33.87	34.61	36.54	34.89	35.30	37.89	33.46	34.42
		SSIM	0.7127	0.9553	0.9703	0.9649	0.9273	0.9586	0.9593	0.9354	0.9531	0.9263
	CLIPDenoising* [7]	PSNR	34.79	37.54	36.30	38.01	40.09	38.74	39.56	42.94	35.50	38.16
		SSIM	0.8982	0.9794	0.9809	0.9771	0.9685	0.9715	0.9769	0.9824	0.9707	0.9672
Ours	Xformer-ours	PSNR	38.98	38.67	37.73	40.22	42.04	39.79	40.61	44.26	36.23	39.84
		SSIM	0.9549	0.9852	0.9857	0.9857	0.9816	0.9773	0.9805	0.9879	0.9748	0.9792

Table S.2. Quantitative comparisons with state-of-the-art generalization methods on the SIDD validation set and multiple real-noise benchmarks. We present the results in terms of PSNR \uparrow (dB) and SSIM \uparrow . Methods marked with a dagger (\dagger) indicate evaluations performed on reproduced models under standardized conditions.

Baseline	Generalization	Metric	In-distribution				Out-of-distribution					
			SIDD	Poly	CC	HighISO	iPhone	Huawei	OPPO	Sony	Xiaomi	OOD Avg.
NAFNet [6]	None	PSNR	39.88	37.13	35.81	38.27	40.16	37.68	39.57	43.48	34.97	38.38
		SSIM	0.9594	0.9714	0.9809	0.9784	0.9700	0.9676	0.9781	0.9824	0.9681	0.9746
	+ AFM \dagger [29]	PSNR	39.83	<u>37.28</u>	<u>36.31</u>	<u>38.40</u>	39.68	<u>38.21</u>	<u>39.84</u>	43.31	<u>35.39</u>	<u>38.55</u>
		SSIM	0.9592	0.9696	<u>0.9815</u>	0.9783	0.9545	<u>0.9683</u>	<u>0.9788</u>	0.9637	<u>0.9709</u>	0.9707
	+ LAN \dagger [12]	PSNR	39.88	37.17	35.59	38.21	40.48	37.53	39.42	<u>43.66</u>	34.83	38.36
		SSIM	0.9594	<u>0.9792</u>	0.9808	<u>0.9787</u>	<u>0.9766</u>	0.9680	0.9773	0.9883	0.9667	<u>0.9770</u>
	+ Ours	PSNR	39.17	38.67	37.82	39.94	41.94	39.74	40.45	44.17	36.14	39.86
		SSIM	0.9566	0.9851	0.9876	0.9853	0.9805	0.9778	0.9796	<u>0.9869</u>	0.9745	0.9822

B. Additional experimental results

B.1. Comparison with additional denoising methods

Table S.1 presents quantitative comparisons between additional image denoising methods and our approach. Generation-based methods such as DANet [34], C2N [11], and PNGAN [4] utilize the SIDD dataset for training, focusing on synthetic-to-real noise generation. MaskDenoising [5] is trained solely on Gaussian noise ($\sigma = 15$), leading to notably poor performance on real-world noise datasets. CLIPDenoising [7] leverages the CLIP encoder and incorporates additional training on synthetic noise generated using Poisson-Gaussian models for sRGB denoising. However, none of these methods outperform our approach across most benchmarks, underscoring the efficacy of our noise translation framework in handling real-world noise scenarios.

B.2. Comparison with generalization methods

Table S.2 showcases results from our reproduction of the AFM [29] and LAN [12] methods using their officially released code, in combination with NAFNet, to enable a direct comparison with our proposed method. Applying LAN to other denoising architectures from our experiments, such as Restormer [36], KBNNet [42], and Xformer [38], was infeasible due to excessive memory demands of LAN when processing images with resolutions exceeding 512×512 . Additionally, our reproduction experiments revealed that LAN’s adaptation methodology not only requires substantial computational resources but also fails to improve generalization performance at resolutions exceeding 256×256 . In contrast, our noise translation framework consistently delivers robust and superior generalization performance across diverse out-of-distribution (OOD) benchmarks, outperforming both AFM and LAN.

Table S.3. Extended full table of Table 4 in the main paper.

$D_{\theta^*} - test$	$D_{\theta^*} - train$	Metric	In-distribution			Out-of-distribution						
			SIDD	Poly	CC	HighISO	iPhone	Huawei	OPPO	Sony	Xiaomi	OOD Avg.
Restormer	Restormer	PSNR	39.08	38.74	37.60	40.06	41.62	39.68	40.55	44.12	36.14	39.81
		SSIM	0.9558	0.9846	0.9861	0.9851	0.9751	0.9761	0.9794	0.9849	0.9747	0.9807
	NAFNet	PSNR	39.19	38.64	37.28	39.94	41.94	39.63	40.51	43.99	36.10	39.75
		SSIM	0.9567	0.9851	0.9859	0.9851	0.9816	0.9767	0.9798	0.9874	0.9743	0.9820
	KBNet	PSNR	38.99	38.57	37.01	39.82	41.62	39.60	40.47	43.75	36.03	39.61
		SSIM	0.9555	0.9841	0.9849	0.9844	0.9755	0.9760	0.9790	0.9842	0.9736	0.9809
	Xformer	PSNR	39.11	38.71	37.79	40.07	41.60	39.61	40.42	44.10	36.16	39.81
		SSIM	0.9559	0.9851	0.9865	0.9850	0.9771	0.9759	0.9797	0.9863	0.9745	0.9813
NAFNet	Restormer	PSNR	39.07	38.55	37.92	39.99	41.63	39.67	40.31	43.64	36.21	39.74
		SSIM	0.9558	0.9834	0.9873	0.9852	0.9755	0.9776	0.9789	0.9821	0.9748	0.9806
	NAFNet	PSNR	39.17	38.67	37.82	39.94	41.94	39.74	40.45	44.17	36.14	39.86
		SSIM	0.9566	0.9851	0.9876	0.9853	0.9805	0.9778	0.9796	0.9869	0.9745	0.9822
	KBNet	PSNR	39.07	38.62	37.60	39.84	41.68	39.77	40.45	44.01	36.07	39.76
		SSIM	0.9559	0.9842	0.9871	0.9848	0.9759	0.9779	0.9793	0.9842	0.9740	0.9809
	Xformer	PSNR	39.04	38.64	38.01	40.07	41.91	39.74	40.48	44.07	36.19	39.89
		SSIM	0.9559	0.9849	0.9876	0.9854	0.9790	0.9774	0.9798	0.9855	0.9746	0.9818
KBNet	Restormer	PSNR	39.02	38.54	37.72	40.13	41.55	39.73	40.46	43.82	36.22	39.77
		SSIM	0.9557	0.9830	0.9856	0.9851	0.9725	0.9773	0.9796	0.9818	0.9752	0.9800
	NAFNet	PSNR	39.15	38.63	37.71	39.94	41.91	39.71	40.49	44.20	36.12	39.84
		SSIM	0.9565	0.9849	0.9865	0.9852	0.9801	0.9775	0.9798	0.9865	0.9744	0.9819
	KBNet	PSNR	39.06	38.57	37.59	39.83	41.63	39.71	40.46	44.04	36.04	39.73
		SSIM	0.9559	0.9840	0.9859	0.9845	0.9752	0.9773	0.9794	0.9839	0.9739	0.9805
	Xformer	PSNR	39.05	38.64	37.76	40.11	41.76	39.70	40.51	44.05	36.21	39.84
		SSIM	0.9558	0.9846	0.9859	0.9852	0.9777	0.9770	0.9802	0.9847	0.9749	0.9813
Xformer	Restormer	PSNR	39.04	38.55	37.71	40.19	41.98	39.67	40.48	44.05	36.27	39.86
		SSIM	0.9556	0.9849	0.9852	0.9861	0.9811	0.9775	0.9800	0.9874	0.9754	0.9822
	NAFNet	PSNR	39.02	38.57	37.65	40.13	42.00	39.74	40.46	44.01	36.14	39.84
		SSIM	0.9555	0.9850	0.9853	0.9858	0.9818	0.9776	0.9799	0.9878	0.9747	0.9822
	KBNet	PSNR	39.02	38.51	37.46	39.98	41.96	39.70	40.46	43.92	36.07	39.76
		SSIM	0.9554	0.9847	0.9850	0.9851	0.9813	0.9775	0.9797	0.9873	0.9741	0.9818
	Xformer	PSNR	38.98	38.67	37.73	40.22	42.04	39.79	40.61	44.26	36.23	39.94
		SSIM	0.9549	0.9852	0.9857	0.9857	0.9816	0.9773	0.9805	0.9879	0.9748	0.9824

B.3. Expanded Table: Adaptability of the Noise Translation Network

Table S.3 extends the results of Table 4 in the main paper, analyzing various combinations of denoising networks used during the training and inference phases within our framework. In this context, $D_{\theta^*} - test$ refers to the pretrained denoising network utilized during inference, while $D_{\theta^*} - train$ denotes the pretrained denoising network employed for training the noise translation network. For instance, when $D_{\theta^*} - test$ is NAFNet and $D_{\theta^*} - train$ is KBNet, the noise translation network is trained to map real-world noise to align with KBNet’s prior but is evaluated with NAFNet during inference. Notably, when $D_{\theta^*} - test$ and $D_{\theta^*} - train$ correspond to different pretrained denoising models, our framework maintains high performance by effectively translating noise distributions to align with the priors of the inference model. This adaptability implies that as new denoising architectures are introduced, they can be seamlessly incorporated into our framework, potentially achieving even greater performance improvements without the need to retrain the noise translation network. Such flexibility ensures the practical applicability of our noise translation framework in real-world scenarios.

B.4. Expanded Table: Gaussian Injection Block and Explicit Noise Translation Loss

Table S.4 provides the complete results for the OOD benchmarks in Table 3 of the main paper. These results further demonstrate the effectiveness of the Gaussian injection block and explicit noise translation loss within the proposed framework.

Table S.4. Effects of using Gaussian noise injection and explicit noise translation loss.

	Metric	In-distribution		Out-of-distribution							
		SIDD	Poly	CC	HighISO	iPhone	Huawei	OPPO	Sony	Xiaomi	OOD Avg.
Baseline Translation	PSNR	39.35	38.32	37.25	39.22	40.80	39.24	39.75	43.86	35.74	39.27
	SSIM	0.9573	0.9820	0.9864	0.9794	0.9700	0.9727	0.9745	0.9857	0.9683	0.9774
+ Gaussian Noise Injection	PSNR	39.05	38.54	37.58	39.79	41.53	39.68	40.40	43.89	36.00	39.61
	SSIM	0.9556	0.9835	0.9866	0.9844	0.9737	0.9773	0.9790	0.9827	0.9737	0.9801
+ Explicit Noise Translation Loss	PSNR	39.37	37.91	37.16	39.07	40.28	37.85	39.06	42.72	35.21	38.66
	SSIM	0.9574	0.9791	0.9862	0.9783	0.9650	0.9613	0.9670	0.9789	0.9605	0.9720
+ Both (Ours)	PSNR	39.17	38.67	37.82	39.94	41.94	39.74	40.45	44.17	36.14	39.86
	SSIM	0.9566	0.9851	0.9876	0.9853	0.9805	0.9778	0.9796	0.9869	0.9745	0.9822

Table S.5. Quantitative comparisons of real-world denoising performance across various training set configurations. Methods marked with an asterisk (*) are evaluated using official out-of-the-box models.

Denoising network	Trained noise	Metric	SIDD	Poly	CC	HighISO	iPhone	Huawei	OPPO	Sony	Xiaomi	Total Avg.
Restormer [36]	SIDD*	PSNR	39.93	37.63	36.31	38.24	40.05	38.36	39.49	44.02	35.62	38.85
		SSIM	0.9598	0.9790	0.9805	0.9753	0.9727	0.9671	0.9768	0.9889	0.9706	0.9745
	SIDD + Gaussian	PSNR	39.67	37.61	35.52	38.08	40.38	38.51	39.83	43.72	35.54	38.76
		SSIM	0.9586	0.9800	0.9771	0.9765	0.9748	0.9690	0.9795	0.9865	0.9714	0.9748
	Ours	PSNR	39.08	38.74	37.60	40.06	41.62	39.68	40.55	44.12	36.14	39.73
		SSIM	0.9558	0.9846	0.9861	0.9851	0.9751	0.9761	0.9794	0.9849	0.9747	0.9779
NAFNet [6]	SIDD*	PSNR	39.88	37.13	35.81	38.27	40.16	37.68	39.57	43.48	34.97	38.55
		SSIM	0.9594	0.9714	0.9809	0.9784	0.9700	0.9676	0.9781	0.9824	0.9681	0.9729
	SIDD + Gaussian	PSNR	39.61	37.93	36.10	38.20	40.66	37.92	39.66	43.49	35.65	38.80
		SSIM	0.9582	0.9809	0.9797	0.9788	0.9779	0.9704	0.9815	0.9886	0.9716	0.9764
	Ours	PSNR	39.17	38.67	37.82	39.94	41.94	39.74	40.45	44.17	36.14	39.78
		SSIM	0.9566	0.9851	0.9876	0.9853	0.9805	0.9778	0.9796	0.9869	0.9745	0.9793

Table S.6. Quantitative results of applying noise translation framework to denoising model pre-trained on pure Gaussian.

Denoising methods	Metric	SIDD	Poly	CC	HighISO	iPhone	Huawei	OPPO	Sony	Xiaomi	Total Avg.
Restormer-Gaussian [36]	PSNR	23.99	35.97	33.41	35.31	38.02	36.94	37.84	42.90	34.49	35.43
	SSIM	0.4990	0.9585	0.9563	0.9464	0.9448	0.9502	0.9629	0.9831	0.9554	0.9063
+ Ours	PSNR	39.08	37.88	35.75	39.33	41.21	38.44	39.96	43.18	35.63	38.94
	SSIM	0.9542	0.9832	0.9800	0.9827	0.9823	0.9719	0.9790	0.9835	0.9720	0.9765

B.5. Comparison with naïve combination of real and synthetic dataset for training

We compare our method with the naïve approach of combining Gaussian noise dataset with the SIDD dataset for training. The results are presented in Table S.5. The Gaussian noise dataset used in this comparison is identical to the one which is used for our method. The results demonstrate that naively combining real-noise and Gaussian noise datasets during training does not yield significant improvements in generalization performance. This highlights the superiority and efficacy of our method in enhancing denoising performance across diverse noise distributions.

B.6. Incorporating a pure Gaussian pretrained denoising network

We conduct an experiment on the officially published denoising model, Restormer [36], which was trained for blind gaussian noise removal. By leveraging it in our framework, we trained the corresponding noise translation network with the proposed methodology to evaluate the overall performance. The results are provided in Table S.6, which demonstrate that even when using a pure Gaussian pretrained out-of-the-box model within our framework, the real-world denoising performance undergoes significant improvement. This enhancement can be attributed to our noise translation network, which effectively adapts the real-world noise into a form closer to the Gaussian noise that the pretrained model is adept at handling. Note that, in our

Table S.7. Sensitivity results on various hyperparameters in our framework.

Pretraining Level			Noise Injection Level			Explicit Loss Weight			Spatial-Frequency Ratio		
σ	SIDD	OOD Avg.	$\tilde{\sigma}$	SIDD	OOD Avg.	α	SIDD	OOD Avg.	β	SIDD	OOD Avg.
5	39.37	38.96	0	39.37	38.66	0	39.05	39.61	0	39.10	39.78
10	39.29	39.64	1	39.33	39.24	0.001	39.03	39.65	0.001	39.15	39.82
15	39.17	39.86	5	39.17	39.66	0.005	39.07	39.72	0.002	39.17	39.86
20	38.88	39.53	15	39.08	39.77	0.01	39.09	39.76	0.005	39.07	39.82
25	38.73	39.21	50	39.11	39.80	0.05	39.17	39.86	0.01	39.07	39.56
			100	39.17	39.86	0.1	39.05	39.67	0.02	39.07	38.97
			200	39.05	39.70	0.5	38.90	37.80	0.05	38.57	37.41

pretraining approach, the denoising network is trained on Gaussian noise augmented with the same real-world noise used to train the noise translation network. This distinction in pretraining strategies explains the observed performance gap between the two results.

B.7. Effects of hyperparameters

Table S.7 presents the ablative results of our hyperparameters, including pretraining noise level (σ), noise injection level ($\tilde{\sigma}$), explicit loss weight (α), and spatial frequency ratio (β). The pretraining level part of Table S.7 shows the ablation results for the Gaussian noise levels added to create noisy input during denoising network pretraining. As the noise level increased, the performance on in-distribution (ID) consistently decreased. For out-of-distribution (OOD), the performance improved until noise level of 15, beyond which it began to degrade, due to oversmoothing effects caused by learning to handle strong noise. The noise injection level part presents the ablation results for Gaussian noise injection levels. Increasing the noise level led to a decline in ID performance, while OOD performance improved up to a certain point. The explicit loss weight and spatial-frequency ratio parts show the ablation results for the α and β values in Eq. (12) and (10), respectively. Overall, the ablation experiments determined the optimal hyperparameters as follows: a pretraining noise level $\sigma = 15$, a Gaussian noise injection level $\tilde{\sigma} = 100$, $\alpha = 5 \times 10^{-2}$, and $\beta = 2 \times 10^{-3}$.

B.8. Training Stability

To evaluate the stability of training our noise translation network, we conducted five independent training runs using different random seeds and measured the PSNR metrics across multiple datasets. The standard deviations for each dataset were as follows: SIDD (0.023), Poly (0.007), CC (0.021), HighISO (0.009), iPhone (0.008), Huawei (0.010), OPPO (0.016), Sony (0.022), and Xiaomi (0.020). The average standard deviation across all datasets was 0.013, confirming the robustness and stability of training with our framework.

C. Qualitative Analysis

C.1. Additional OOD datasets and SIDD

Qualitative results on all datasets in the main paper are shown in Figures S.1 and S.2. Our method significantly surpasses the PSNR scores of other denoising models on all OOD datasets (iPhone, Huawei, OPPO, Sony, Xiaomi). Notably, the output images of KBNNet [42], exhibit visible breakdowns due to severe overfitting to the training set. For the in-distribution SIDD, our method produces clean results without generating unnecessary zipper artifacts.

C.2. NIND (Natural Image Noise Dataset)

The NIND [3] dataset comprises high-resolution images captured at various ISO levels. High ISO images are noisier due to increased sensor sensitivity, while low ISO images, though cleaner, may require more optimal settings or equipment to capture effectively. Figure S.3 and Figure S.4 illustrate the qualitative results of our method applied to high ISO images, demonstrating its ability to effectively remove noise while preserving fine image details. The denoised outputs are visually clean and free from artifacts, achieving a quality comparable to images captured at low ISO levels.

C.3. Real-world smartphone image noise and denoising results

Finally, we present the denoised results of images captured using our Galaxy S22+ smartphone, as shown in Figure S.5.

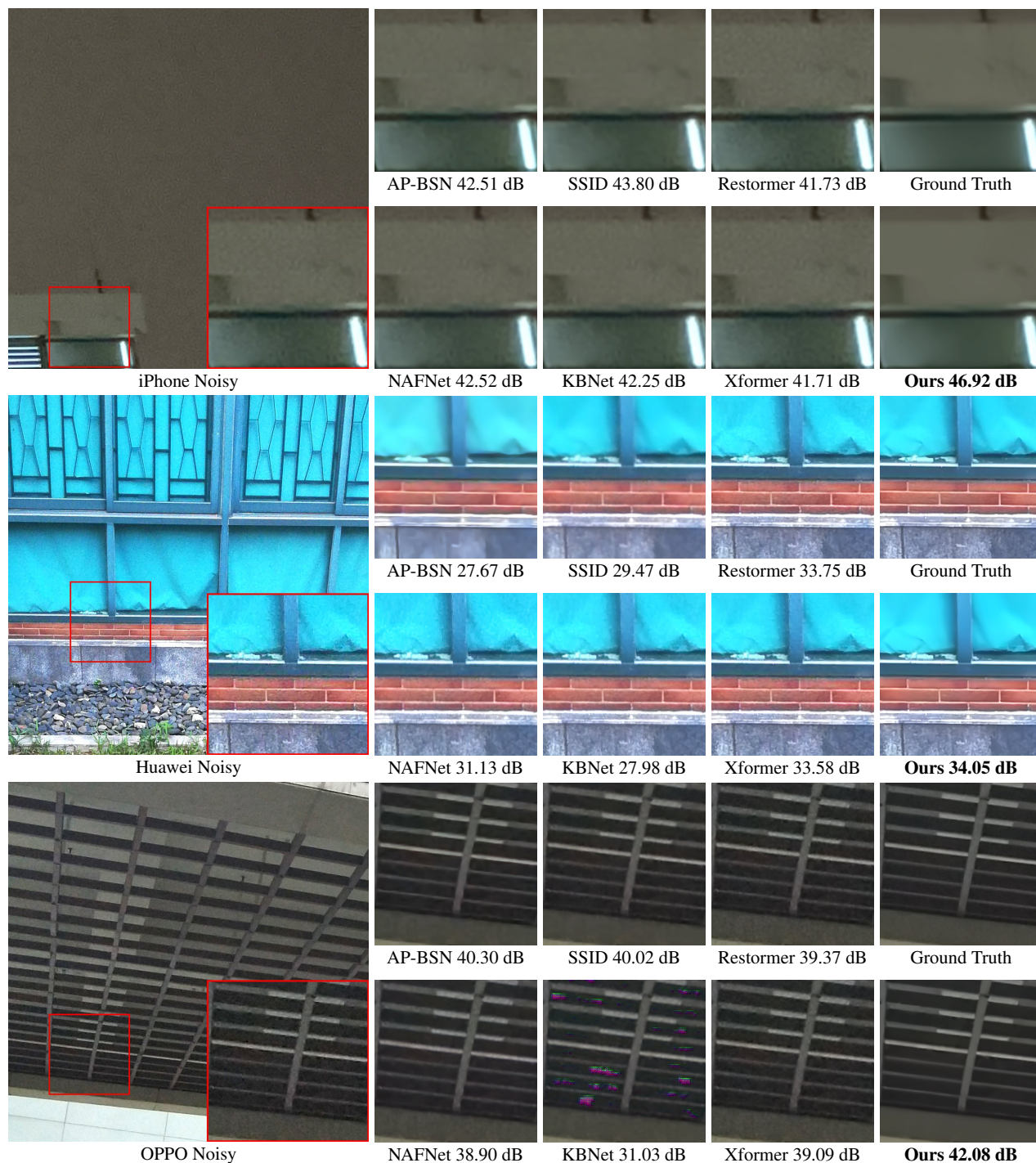


Figure S.1. Comparison between the qualitative results of various denoising networks including ours (noise translation network with pretrained NAFNet) on iPhone, Huawei, and OPPO dataset. Zoom in for a closer inspection of the visual quality.

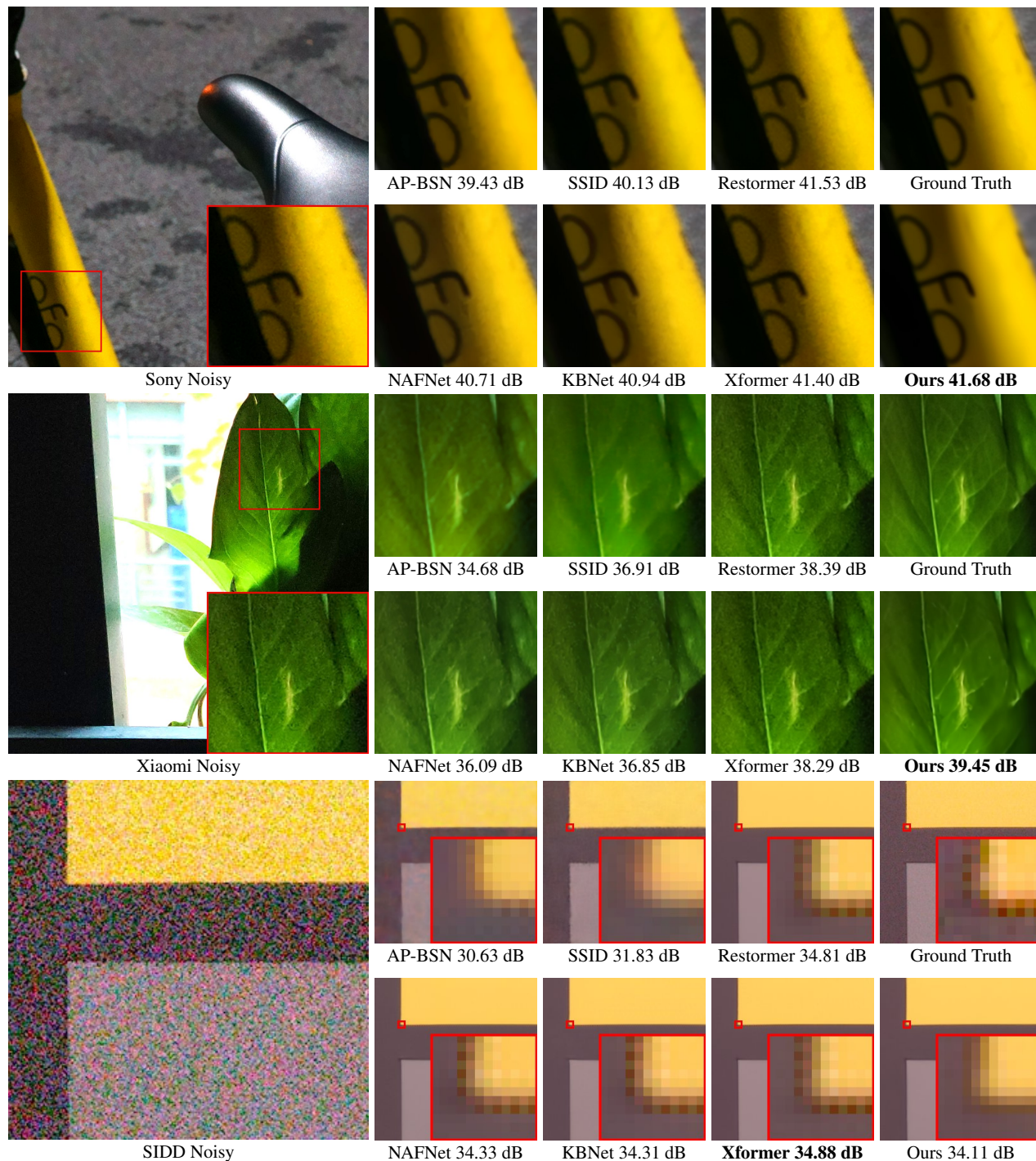


Figure S.2. Comparison between the qualitative results of various denoising networks including ours (noise translation network with pretrained NAFNet) on Sony, Xiaomi, and SIDD datasets. Zoom in for a closer inspection of the visual quality.

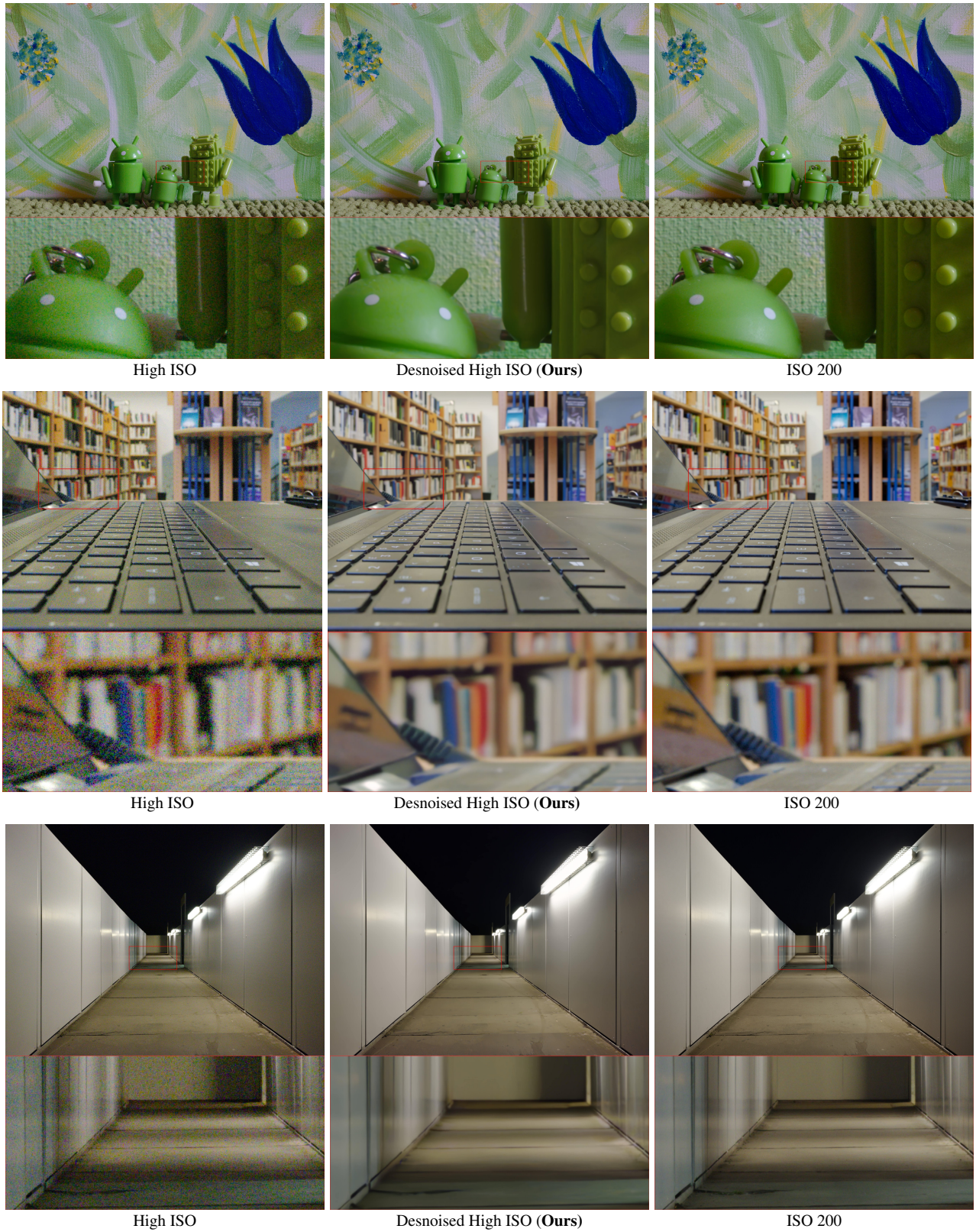
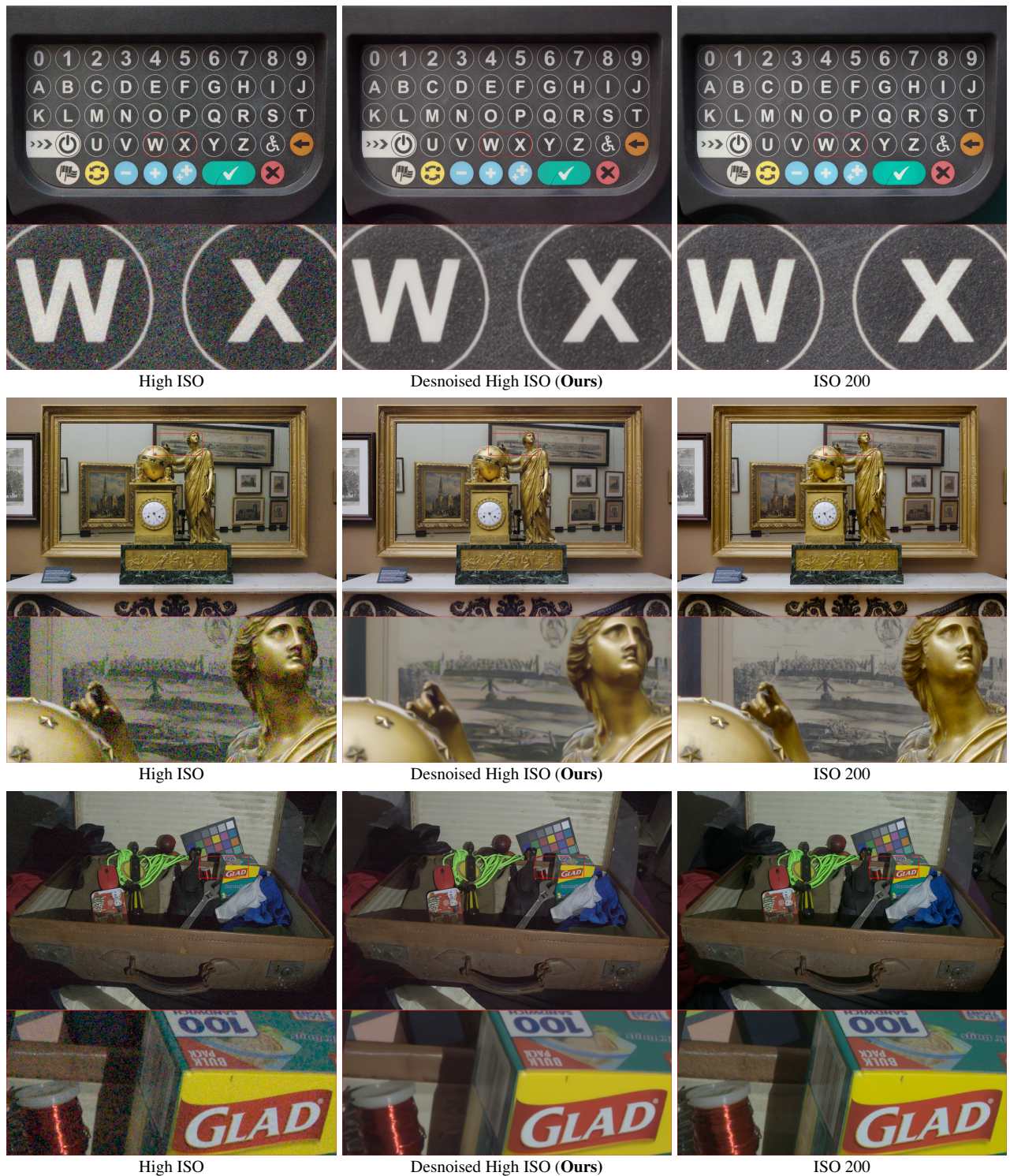


Figure S.3. Qualitative results of our noise translation network with pretrained NAFNet applied to high ISO images from the NIND dataset. Our method effectively removes noise while preserving fine details, producing outputs comparable to low ISO (ISO 200) images. Zoom in for a closer inspection of the visual quality.



High ISO

Desnoised High ISO (Ours)

ISO 200

High ISO

Desnoised High ISO (Ours)

ISO 200

High ISO

Desnoised High ISO (Ours)

ISO 200

Figure S.4. Qualitative results of our noise translation network with pretrained NAFNet applied to high ISO images from the NIND dataset. Our method effectively removes noise while preserving fine details, producing outputs comparable to low ISO (ISO 200) images. Zoom in for a closer inspection of the visual quality.

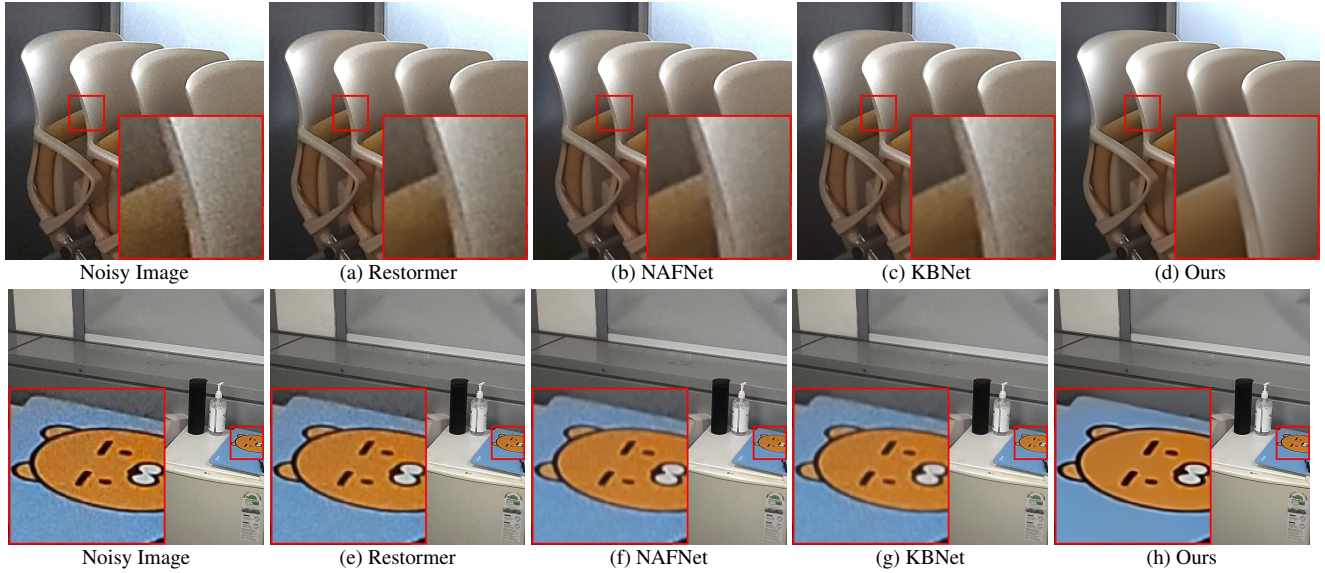


Figure S.5. Comparison between the qualitative results of various denoising networks including ours (noise translation network with pretrained NAFNet) on images captured by Galaxy S22+ smartphone. Zoom in for a closer inspection of the visual quality.

D. Reproducibility Statement

To ensure reproducibility of our work, we have made efforts to include key details in the main text and appendix. Furthermore, we provide the complete source code and model weights in the supplementary material to facilitate easy reproduction of the experiments and results.